Broadband Acoustic Communication Aided Underwater Inertial Navigation System

Jae Won Choi, *Graduate Student Member, IEEE*, Aseem V. Borkar, Andrew C. Singer, and Girish Chowdhary, *Senior Member, IEEE*

***Abstract*—We present an underwater localization system for medium-sized Autonomous Underwater Vehicles (AUVs) that leverages a broadband wireless acoustic communication system for GPS-denied underwater localization. Many current acoustic localization systems assume a single line-of-sight path and use either narrow-band signals or short-duration pings for the convenience of mitigating motion-induced Doppler at the expense of the time-of-arrival (TOA) accuracy and operational flexibility. We propose a novel acoustic localization system that utilizes the aggressive signal processing embedded in underwater acoustic communication systems to resolve multi-path and Doppler distortion and finely estimate timing information using broadband communication signals. Timing and Doppler information extracted from this process is then used to estimate biases and drift from an inertial navigation system (INS) using a Bayesian framework. To demonstrate the feasibility of the system model, co-simulations are created from the MACE10 experimental data. Our results show dramatic improvement in localization accuracy, with an error of less than 120 m achieved over the 3∼7 km distance range from the MACE 10 experiment between an AUV and a remote beacon with an acoustic communication transmission interval of 30 seconds.**

***Index Terms*—Localization, marine robotics.**

I. Introduction

AUTONOMOUS navigation for autonomous underwater vehicles (AUV) remains a major engineering challenge, primarily because GPS-based localization is not possible underwater to determine the position of the AUV. Pose estimation without GPS or another position correction mechanism is challenging, because inertial measurement unit (IMU) measurements drift, and there is little in the way of landmarks to navigate in deep waters. In the underwater environment where radio-frequency waves are evanescent (and do not propagate beyond a skin-depth into the water), an acoustic signal from a beacon of known location can be used in a fashion similar in spirit to a GPS signal from a satellite. The propagation delay (or TOA) of an acoustic signal can be used as a distance measurement, which can correct for the time-integration error in an IMU. However, due to the physical characteristics of underwater acoustics, an acoustic signal at the receiver is corrupted by time-varying multi-path propagation and motion-induced Doppler, making TOA estimation a challenge. There have been successful efforts in the underwater acoustic communication literature [1], [2], and [3], leveraging aggressive signal processing to find, track, and exploit this time-varying multi-path and Doppler distortion to recover transmitted communication signals. Once estimated, the Doppler effects can serve as valuable information for localization since the instantaneous Doppler factor from the acoustic beacon can be modeled as a relative velocity between the beacon and AUV. While there have been other localization schemes using Doppler measurements from communication signals [4], [5], the focus has been using narrow-band signals to measure Doppler through estimating an instantaneous frequency shift. Although a narrow-band signal is convenient for estimating the Doppler factor, its performance on TOA estimation (and its time-resolution generally) is worse than that from a signal using wider bandwidth, which is characterized by the inverse of the signal bandwidth [6]. On the other hand, using broadband signals adds complexity in resolving the Doppler factor because the motion-induced Doppler introduces time-scale distortion and cannot simply be modeled as a frequency shift, as in the narrow-band case.

The main contribution of this letter is incorporating the signal processing technique of [7] that allows accurate TOA and Doppler estimation from broadband communication signals under time-varying Doppler and multi-path effects into an inertial navigation system model via a Bayesian filtering framework. The technique introduced in this letter enables timing information extraction from broadband communication signals, opening the possibility for more accurate TOA estimation [6] as compared to the narrow-band model generally in use for localization today. To our knowledge, we are the first to use broadband acoustic communication signals for a ranging system that exploits the extensive signal processing in the acoustic communication community for Doppler and multi-path mitigation. Without additional computation to our existing communication scheme, the timing information (Doppler factor and TOA) is given as a byproduct of the Doppler compensated decision feedback equalizer (DFE). Then, extracted timing information is translated into distance and velocity measurements, which are used to correct for IMU noise and bias errors integrated

Manuscript received September 9, 2021; accepted January 30, 2022. Date of publication February 24, 2022; date of current version March 11, 2022. This letter was recommended for publication by Associate Editor F. Zhang and Editor P. Pounds upon evaluation of the reviewers' comments. This work was supported in part by the University of Illinois Urbana-Champaign College of ACES Future Interdisciplinary Research Explorations (FIRE) Award Signals in the Soils and Signals Through the Soils, ONR under Grant N0004-12-1-2662 and in part by TechnipFMC Educational Fund Fellowship. *(Corresponding author: Jae Won Choi.)*

The authors are with the Coordinate Science Laboratory, University of Illinois Urbana-Champaign, Urbana, IL 61801 USA (e-mail: choi223@illinois.edu; avborkar@illinois.edu; acsinger@illinois.edu; girishc@illinois.edu).

Digital Object Identifier 10.1109/LRA.2022.3154004

over time using a Bayesian filtering framework for accurate estimation of AUV pose. Also, the inertial measurement from the IMU provides coupling among timing information measured at consecutive symbols, providing the capability of localization even under a single beacon scenario, similar to the mechanism of the synthetic long baseline method [8].

The remaining sections of this letter are organized as follows. The next section introduces past work on AUV localization. Section III discusses the navigation and observation model in this work. Then in section IV, a Doppler compensation method from [7] is introduced to extract time-of-arrival and Doppler information from the communication signal and a theoretical bound based on the signal model is explored. Section V covers the filter implementation using the state and observation model discussed in previous sections. Finally, section VI verifies the feasibility of the system using a simulation based on the MACE10 experiment data set.

II. Related Work

Despite an abundance of literature on the different methods used for AUV localization, the problem of underwater pose estimation remains quite open. For a detailed survey of different approaches, we refer the reader to [9] and [10]. In this section, we briefly review different approaches to the underwater localization problem.

Many approaches to underwater pose estimation rely on the use of IMU. Low cost inertial sensors are highly compact and offer an attractive solution for the creation of low-cost AUVs. IMU-based systems do not require *a priori* knowledge about the environmental structure, and hence hold the promise of working across changing bathymetry. However, navigation methods based on the time integration of the inertial measurements, so-called dead reckoning (or ded reckoning), suffer from drift from time integrated measurement bias and error. Such drifts are more prominent in "strapdown" (in other words rigidly affixed) inertial sensors. Thus, IMU-based navigation systems need to be often aided by acoustic ranging systems using hydrophones or transducers. Such methods are relatively inexpensive and robust to environmental changes. However, as discussed in the previous section, there are challenges of measuring accurate timing information from acoustic ranging systems due to multi-path and Doppler effects.

Most acoustic systems use the two-way travel-time (TWTT) between multiple beacons and the AUV to triangulate its position. These schemes are generally classified as long baseline (LBL) [11], short baseline (SBL) [12], ultra short baseline (USBL) [13] and single beacon systems. The LBL methods require the setting up of a network of beacons which is expensive. SBL and USBL methods use a single beacon consisting of an acoustic transceiver array, and estimate relative range and bearing to the AUV, using TWTT and phase difference. But these systems need an active transmitter on the AUV which increases the cost and decreases endurance of the AUV due to the power consumed.

The development of chip-scaled atomic clocks have made localization using one-way travel-time (OWTT) ranging, (with clock synchronization) possible leading to the development of single beacon systems. Range only OWTT navigation has been implemented in [14] where the range derived from the OWTT measurement is fused with dead reckoning via maximum likelihood estimation. Similar experiments are also presented in [15] [16] and [17] using range-only OWTT measurements. This approach utilizes the signal detection preamble of acoustic communication sequence to measure TOA by matched filtering methods [18]. We extend this method to provide a framework that makes use of the entire broadband communication sequence in concert with inertial measurements and can provide updates at a much higher rate - as fast as symbol-by-symbol updates.

A relatively new approach that is related to this letter has been studied in [19], where the authors utilize a communication system to measure Doppler and TOA with the capability of using a wide bandwidth signal. The difference is in both the communication scheme and time-scale of operation, where authors of [19] use a pulse position modulated linear frequency chirp and estimate localized Doppler shifts by detecting peaks in in the frequency domain across relatively-short time intervals, while our method operates on a much finer time-scale. Our approach leverages quadrature amplitude modulation with symbol-by-symbol Doppler factor estimates extracted by estimating the inverse of the time-scale distortion recursively using the phase differences of successive QAM transmitted symbols together with DFE outputs. By use of a DFE, we both address multi-path distortion that was not dealt in previous approaches and which causes other methods to break down as well as provide a much higher update rate.

III. AUV Kinematics and Sensor Model

A. Inertial Navigation

Our goal is to estimate the pose in a local inertial frame in the north, east, and down (NED) coordinate system. For a strapdown IMU, the measurements are taken with respect to the body frame in an xyz coordinate system, with each axis corresponding to forward, right-hand side facing forward, and bottom respectively. The orientation of the vehicle can be represented by a rotation from the inertial frame to the body frame using a unit quaternion, $\mathbf{q} = [q_1\ q_2\ q_3\ q_4]^T$. Also, by defining the body frame angular velocity as $\boldsymbol{\omega}_b = [p\ q\ r]^T$, the first order dynamics of the orientation in quaternion is

$$\dot{\mathbf{q}} = \frac{1}{2}\Omega\mathbf{q}, \tag{1}$$

where

$$\Omega = \begin{bmatrix} 0 & -p & -q & -r \\ p & 0 & r & -q \\ q & -r & 0 & p \\ r & q & -p & 0 \end{bmatrix}. \tag{2}$$

Let $R_{b\to i}$ be the rotation matrix representing rotation from body to inertial frame. Using the rotation matrix, the translation dynamics of the system can be expressed in terms of body frame acceleration, $\mathbf{a}_b$, as $\dot{\mathbf{p}}_i = \mathbf{v}_i$, $\dot{\mathbf{v}}_i = \mathbf{a}_i$, and $\mathbf{a}_i = R_{b\to i}\mathbf{a}_b$,

where $\mathbf{p}_i$, $\mathbf{v}_i$, and $\mathbf{a}_i$ are the position vector, velocity vector, and acceleration vector in the inertial frame, respectively.

The IMU measurements are modeled as additive white noise with a random walk bias. The body frame angular velocity and acceleration are measured by the IMU with the following relationships

$$\boldsymbol{\omega}_b = \tilde{\boldsymbol{\omega}}_b + \mathbf{b}_{\boldsymbol{\omega}_b} + \mathbf{w}_{\boldsymbol{\omega}_b} \tag{3}$$

$$\mathbf{a}_b = \tilde{\mathbf{a}}_b + \mathbf{b}_{\mathbf{a}_b} + \mathbf{w}_{\mathbf{a}_b}. \tag{4}$$

Equation (3) expresses the body frame angular velocity with $\tilde{\boldsymbol{\omega}}_b$, $\mathbf{b}_{\boldsymbol{\omega}_b}$, and $\mathbf{w}_{\boldsymbol{\omega}_b}$ as the measurement, bias and noise of the gyroscope in the IMU. Similarly, body frame acceleration in (4) is modeled with $\tilde{\mathbf{a}}_b$, $\mathbf{b}_{\mathbf{a}_b}$, and $\mathbf{w}_{\mathbf{a}_b}$ as the measurement, bias and noise of the accelerometer.

The proposed system assumes that a depth measurement is available from a barometer, which we model as

$$p_D = \tilde{p}_D + \mathbf{w}_{p_D}, \tag{5}$$

where p_D is the depth in the inertial frame, $\tilde{p}_D$ is the barometer depth measurement, and $\mathbf{w}_{p_D}$ is a noise term comprising error from the sensor and pressure-to-depth conversion.

B. OWTT Acoustic Observation

We assume a OWTT ranging setup with a beacon transmitting at a known fixed pose. In the OWTT setup, the time-of-flight can be directly estimated from the time-of-arrival. The relationship between time-of-flight and range is as follows

$$\tau = \frac{||\mathbf{p}_{rx} - \mathbf{p}_{tx}||}{c}, \tag{6}$$

where $\mathbf{p}_{rx}$ and $\mathbf{p}_{tx}$ are the position of a receiver and a transmitter in an inertial frame and c is the speed of sound, which is assumed constant over the one-way travel path.

The Doppler factor is defined as the first time derivative of the delay τ. Given OWTT and a static transmitter, the Doppler factor can be written in terms of transmitter and receiver poseq and velocity as

$$D = \frac{\langle \mathbf{v}_{rx}, \mathbf{p}_{rx} - \mathbf{p}_{tx} \rangle}{c||\mathbf{p}_{rx} - \mathbf{p}_{tx}||}. \tag{7}$$

Let $\mathbf{p}_{sen}$ be the location of a receiver placed on a vehicle in the body frame, then the $\mathbf{p}_{rx}$ and $\mathbf{v}_{rx}$ are the location and the velocity of a receiver on the inertial frame defined as $\mathbf{p}_{rx} = \mathbf{p}_i + R_{b\to i}\mathbf{p}_{sen}$, and $\mathbf{v}_{rx} = \mathbf{v}_i + R_{b\to i}(\boldsymbol{\omega}_b \times \mathbf{p}_{sen})$.

IV. Acoustic Communication Signals

We consider a wireless communication system for underwater vehicles that makes use of acoustic propagation as the transmission medium, rather than electromagnetic propagation, as in traditional radio-frequency (RF) communication systems. In an acoustic communication system, a carrier signal is generated in much the same way as in RF radio systems. The information bits are represented as a stream of complex quadrature amplitude modulated symbols over a sinusoidal carrier signal. However the carrier is generated using an acoustic transducer and propagates a mechanical pressure wave through an underwater channel

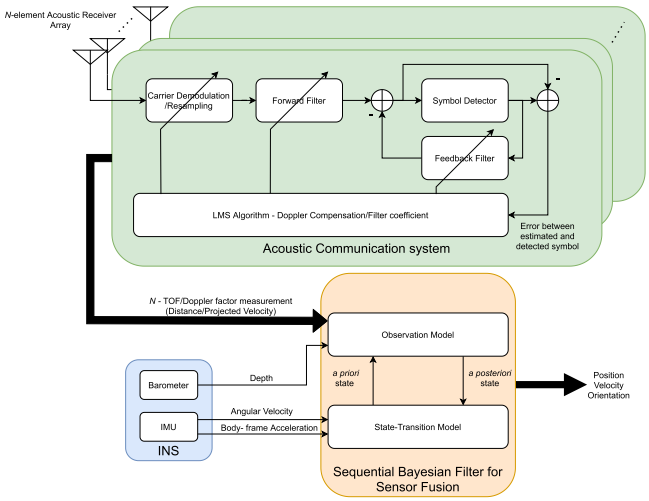

Fig. 1. Block diagram of the Bayesian filter fusing inertial navigation system and communication system. The acoustic communication system is capable of retrieving transmitted signals in an environment with multi-path, and motion-induced Doppler effect. As a byproduct of the Doppler compensator, TOF and Doppler factor measurements from the communication system are fused with inertial navigation sensors using the Bayesian filtering framework.

that poses unique challenges, as opposed to an electromagnetic one. Compared to its electromagnetic counterpart, the acoustic wave propagates five orders of magnitude slower (10^3 vs. 10^8 m/s). Thus the signal is dilated/contracted in time much more severely due to motion-induced Doppler effects. In order to recover transmitted information, the acoustic communication system must estimate the Doppler factor and compensate for the resulting distortion. As the byproduct of the process, we can obtain estimates of the timing and Doppler factor at the time scale of the communication symbols.

Fig. 1 depicts receive-side processing in conjunction with the INS. In order to demodulate the transmitted symbols, the receiver must first correct for frequency shifts and time scaling in the demodulation/resampling block. Then the symbol is estimated using an adaptive DFE, capable of resolving multi-path distortion. In training mode, where transmitted symbols are known, the equalizer filter coefficients and time-scale information is updated using the least mean squares (LMS) algorithm on the error between the estimated output symbol of the DFE and the training symbols. For the data payload, the transmitted symbols are not known to the receiver, so the error is computed in decision-directed mode. Thus, with sufficient signal-to-noise ratio, the proposed method is capable of measuring timing information based on unknown transmitted signals with *a priori* knowledge only of the symbol constellation and a training sequence. The adaptive structure of the DFE, as shown in Fig. 1, has the capability of compensating for multi-path without prior knowledge of the environmental structure beyond a rough estimate of the channel delay spread to parameterize the DFE.

A. Broadband Doppler Compensation

We use the Doppler compensation method presented in [7] to extract the timing information from the communication system.

Let $t_{tx} = \alpha(t_{rx})$ represent the transmission time as a function of the receive time t_{rx}. The main idea behind the Doppler the compensation method of [7] is to recursively estimate the inverse function $\alpha^{-1}()$ for every symbol arrival. Given that symbols are sent at T second intervals, we want to estimate $\alpha^{-1}(nT)$, in short α_n^{-1}, to recover the the timing of the same symbol in the receiver clock. The details of the method are presented in [7]. As the result of the Doppler compensation, we obtain α_n^{-1} and its approximate first order time derivative β_n for every symbol arrival.

From the algorithm, we can extract time-of-flight τ_n and Doppler factor D_n at n-th symbol as

$$\tau_n = \alpha_n^{-1} - nT, \tag{8}$$

$$D_n = 1 - \frac{1}{\beta_n}. \tag{9}$$

These timing measurements are byproducts of the communication system and can be easily extracted without any additional computation other than those required for the existing receiver elements. Also note that α is modeled as a generic function of time and the algorithm is updated every symbol, making the algorithm capable of tracking time-varying Doppler and delay measurements at symbol rates, orders of magnitude finer than prior efforts. These measurements are then translated into a state space model using (6) and (7).

B. Error Bound on the TOA Estimation

Consider a received signal under the channel modeled by stationary motion-induced Doppler, multi-path and additive white Gaussian noise,

$$r(t) = \sum_{i=0}^{L-1} \frac{h^{(i)}}{\sqrt{\beta^{(i)}}} s\left(\beta^{(i)}(t - \tau^{(i)})\right) + \nu(t), \tag{10}$$

where $s(t)$ is the transmitted passband signal, and $\nu(t)$ is a white Gaussian process with flat power spectral density of $N_0/2$. Superscript (i) denotes the multi-path arrivals where $i = 0$ is the first direct path arrival, and $i = L-1$ is the last arrival. $h^{(i)}$, $\beta^{(i)}$ and $\tau^{(i)}$ are gain, time scale, and time delay of the i-th path. For brevity of expression, we will refer to direct path gain, time scale and time delay as h, β and τ for this section. Consider a phase shift keying signal with sinc pulse shaping filter, symbol rate W, and carrier frequency f_c. Then $s(t)$ is modeled as

$$s(t) = \sum_{n=0}^{N-1} \text{sinc}(Wt - n)\cos(2\pi f_c t + \phi_n), \tag{11}$$

with N the length of transmitted symbols and the phase ϕ_n representing the n-th symbol. Following chapter 4.2.3 of [20], the Cramér-Rao lower bound (CRLB) on the mean squared error (MSE) of direct path time delay estimation is derived with (11) and (10) as

$$\begin{aligned}&\text{Var}(\hat{\tau}) \\ &\geq \frac{N_0}{\frac{2h^2}{\beta}\int_{-\infty}^{\infty}\left(\sum_{n=0}^{N-1} 2\pi f_c \beta \text{sinc}_n \sin_n - \beta\pi W \text{sinc}'_n \cos_n\right)^2 dt} \\ &\geq \frac{N_0}{2\beta T_d (h\pi N)^2 (2f_c + W)^2},\end{aligned} \tag{12}$$

where $\cos_n = \cos(2\pi f_c \beta(t-\tau) + \phi_n)$, $\sin_n = \sin(2\pi f_c \beta(t-\tau) + \phi_n)$, $\text{sinc}_n = \text{sinc}(W\beta(t-\tau) - n)$, and $\text{sinc}'_n = \frac{1}{\beta W}\frac{\partial \text{sinc}_n}{\partial t}$. The last inequality is result of $|\text{sinc}_n \sin_n| \leq 1$, $|\text{sinc}'_n \cos_n| \leq 1$ and integration over the transmission duration T_d. Although the lower bound given in (12) approximates the CRLB, it is provided to give perspective on the factors that effect the TOA estimation accuracy. Note that the multi-path gain and time scale factors are nuisance parameters in CRLB formulation for TOA. Intuition behind the CRLB is that the bound is given under the assumption that multi-path and Doppler distortions are compensated without error since the Fisher information is computed given the actual parameter values. Under such circumstances we can observe that a longer signal length, a higher carrier frequency and a wider bandwidth can contribute to lower estimation error. In section VI, the performance of the proposed TOA estimation method is compared with the numerically computed lower bound discussed in this section.

V. Bayesian Filter Formulation

The positioning system is composed of a vehicle with m transducers acting as receivers and n beacons equipped with a single transducer acting as transmitters. Assuming clocks are synchronized, speed of sound is known and constant throughout the space, and beacons are fixed in known positions, measurements (6) and (7) represent distance and velocity projected along the line between the receiver and transmitter. Modeling and measurement errors can readily be treated as measurement noise in the model. For each beacon i and receiver j pair, a time-of-flight $\tau_{i,j}$ and Doppler $D_{i,j}$ measurement is available, making total mn measurements. An advantage of modeling each sensor and beacon measurement separately is the scalability of the model, independent of the sensor setup. The navigation system assumes that an AUV is also equipped with an IMU that measures the angular velocity and the acceleration in the body frame and a barometer that measures the depth of the vehicle. The system equations are described as

$$\dot{\mathbf{x}} = f(\mathbf{x}, \mathbf{u}, \mathbf{w}_f), \tag{13}$$

$$\mathbf{y} = g(\mathbf{x}, \mathbf{u}, \mathbf{w}_g), \tag{14}$$

where $\mathbf{w}_f$ is IMU state transition noise, $\mathbf{w}_g$ is measurement noise, $\mathbf{x}$ is the state vector defined as $\mathbf{x} = \left[\mathbf{p}_i^T\ \mathbf{v}_i^T\ \mathbf{q}^T\ \mathbf{b}_{\boldsymbol{\omega}_b}^T\ \mathbf{b}_{\mathbf{a}_b}^T\right]^T$, $\mathbf{u}$ are measurements from the IMU treated as control inputs defined as $\mathbf{u} = \left[\tilde{\boldsymbol{\omega}}_b^T\ \tilde{\mathbf{a}}_b^T\right]$, and $\mathbf{y}$ is the observation vector containing acoustic measurements and barometer depth measurements, $\tilde{p}_D$, given as $\mathbf{y} = \left[\tilde{\tau}_{0,0}\ \tilde{\tau}_{0,1}\ \cdots\ \tilde{\tau}_{m-1,n-1}\ \tilde{D}_{0,0}\ \tilde{D}_{0,1}\ \cdots\ \tilde{D}_{m-1,n-1}\ \tilde{p}_D\right]^T$. The Doppler measurement model (7) dependends on the angular velocity measurement from the IMU. Hence, (14) contains $\mathbf{u}$ as a input.

Since the acoustic communication symbol rate is much faster than the IMU sampling rate, the acoustic measurements are averaged over the IMU sampling intervals to match their processing rates. For implementation, the system equations are discretized over the IMU measurement intervals, and the observation vector includes the measurement that is currently available at the time. To solve the state space equations recursively, we use an extended kalman filter (EKF), linearized about the current mean and covariance of the estimated state, and a particle filter (PF), an asymptotically optimal nonlinear Bayesian filter as the number of particles goes to infinity (high computational complexity). Although the unscented Kalman filter, a more recent nonlinear variant of the Kalman filter compared to the EKF, has been shown to outperform the EKF in many scenarios [21], constraints on the rotation quaternion imposes a challenge in accurate sigma point computation for the unscented Kalman filter. The diagram in Fig. 1 shows the overall system integration architecture of the communication system and INS using a Bayesian filtering framework, such as an EKF and PF.

VI. Experiments

We performed experiments in simulation with real-world data from the MACE10 experiment. The original goal of this experiment was to gather data for use in mobile MIMO acoustic communications methods. The experiment was conducted in June 2010, approximately 100 km south of Martha's Vineyard, in Massachusetts. An acoustic transmitter array was towed along a rough rectangular track approximately 400 m north-south and 3.8 km east-west at speeds of up to 3 knots. A 12 channel receiver array was moored at a depth of approximately 50 m and is located 3 km in its closest point and 7 km in its furthest point from the track. The experiment was repeated for 3 days, and accumulated approximately 6 hours of communication data in total.

The MACE10 data set also includes the ship data on its position and velocity measured by on-board GPS. The ship data are recorded at one minute intervals for all of the days that the experiment was conducted.

For our emulation of experimental data, we constructed IMU measurements as if located on the towed source and as if the towed source array were mounted on an autonomous underwater vehicle. The parameter values for the model are taken from the datasheet of ADIS16470 MEMS IMU from Analog Devices. The noise densities for the accelerometer and the gyroscope are $100\ \mu\text{g}/\sqrt{\text{Hz}}$ and $0.008^\circ/\text{s}/\sqrt{\text{Hz}}$ and in-run bias stabilities are $13\ \mu\text{g}$ and $0.00022^\circ/s$. These IMU measurements are emulated assuming that the measurement noises are white, Gaussian and independent for each axis. The biases for the accelerometer and gyroscope are assumed to have Gaussian random walk behavior, which are known to be reasonable assumptions for the IMU types considered [22].

For the acoustic measurements, we used statistics recovered from the MACE10 experiment. The acoustic communication signals were sent every four minutes in five seconds segments. The transmission was a single input multiple output configuration with QPSK symbols at 9.765 kHz symbol rate and 13 kHz carrier frequency. Using the MACE10 data set, results

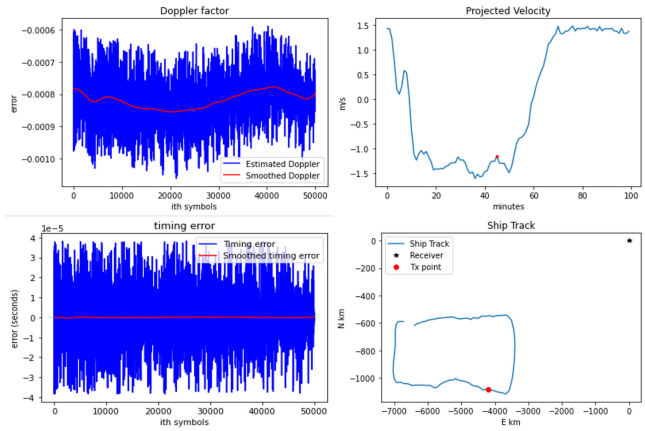

Fig. 2. Doppler (upper-left) and timing (lower-left) estimates from a communication packet in MACE10. Projected velocity (upper-right) and location (lower-right) of the ship during the transmission taken from the ship log.

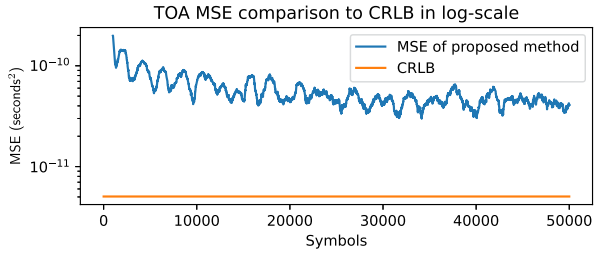

Fig. 3. MSE of TOA estimation given by the Doppler compensated DFE compared to the CRLB.

in [3], and [7] successfully recovered communication signals and showed that the estimated Doppler factor matches the projected velocity of the ship. Using the Doppler compensated DFE algorithm, symbol timing and Doppler factor were estimated for this letter. Fig. 2 shows the Doppler and timing measurement of a single transmission packet taken from the experiment, and the ship position and velocity data corresponding to the timestamp that the communication packet was sent. From the same packet, MSE of timing estimation is compared to the CRLB in Fig. 3. The CRLB is numerically computed using (12) with the entire transmission sequence assuming fixed Doppler factor $D = -8 \times 10^{-4}$ as estimated by the Doppler compensator. The MSE is computed empirically with 1000 most recent symbols. We observe that the TOA error is showing a decreasing trend towards the lower bound as the number of the symbols received increases. However, a gap between the lower bound and the MSE exists, in part because the estimation algorithm is sub-optimal, and the multi-path and Doppler effects are not stationary in the real data. The noise statistics are obtained by subtracting out the smoothed value from the estimated value. The RMSE values of the extracted symbol timing and Doppler factor are $6.257\ \mu s$ and 3.233×10^{-5} respectively. The simulation is based on 84 minutes worth of the data collected during the last day of the experiment. The NED inertial frame origin is defined by the location of the moored receiver. Longitude and latitude measurements from GPS ship data are converted to the NED-coordinate by assuming a flat surface (neglecting Earth curvature) over the

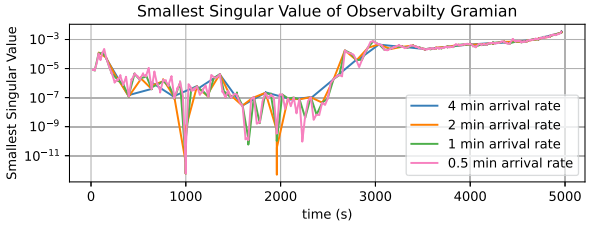

Fig. 4. Smallest singular value of local observability Gramian matrices at the time of communication signal reception.

region of interest. This assumption is reasonable since the area covered by the vehicle is sufficiently small. The position and velocity points from the ship data are interpolated and smoothed to create "ground truth" for the simulated AUV dynamics. While the AUV is running through the rectangular path, the IMU simulator samples the body frame acceleration and angular velocity at 100 Hz with the dynamic model described in the section III, which serves as control input to the Bayesian filter framework.

Assuming a symmetric communication channel, the transmission beacon of known location is placed in the position of the moored receiver array in the MACE10 experiment. The simulated AUV is equipped with 4 acoustic receivers located at $[1, 0, -1]^T$m, $[1, 0, 1]^T$m, $[-1, -1, 0]^T$m, and $[-1, 1, 0]^T$m in AUV body frame coordinates. We have chosen a different receiver array configuration than the straight-line array configuration used in the experiment because of observability issues that arise with the original configuration. Time-of-arrival and Doppler measurements are corrected for the array geometry differences between the experiment and simulation.

As for the initial condition setting in EKF, we assumed that the position information is Gaussian distributed with mean at its true position and covariance of 5 m. Such an assumption is reasonable since an AUV in practical scenarios can obtain its initial position from the surface through GPS.

The original experiment suffers from 4 minute absences of the acoustic measurements in between each acoustic transmission. To observe the effect of the duration of silence in between the acoustic transmission segments, we simulated different silence intervals by dividing the communication signal into multiple pieces distributed uniformly throughout the transmission time. We have experimented with 4 different configurations, where each transmission segment is divided into 1, 2, 4, and 8 segments. For each, the acoustic transmission arrives every 4, 2, 1, and 0.5 minutes. Local observability of the system is plotted in Fig. 4 which shows smallest singular value of observability Gramian matrices of the linearized model along the vehicle's trajectory. Since the system model is a non-linear function of states, observability of the system is analyzed by linearizing the equation over a short duration when the acoustic signal is available to the vehicle [23]. For each 0.1 s segment of acoustic signal reception, the observabilty Gramian is computed by linearizing the model along the ground truth. Figs. 5 and 7 show the performance of the EKF for each transmission interval. Given that the distance between the beacon and the vehicle ranges from 3 to 7 km, the performance of the EKF is within a reasonable range.

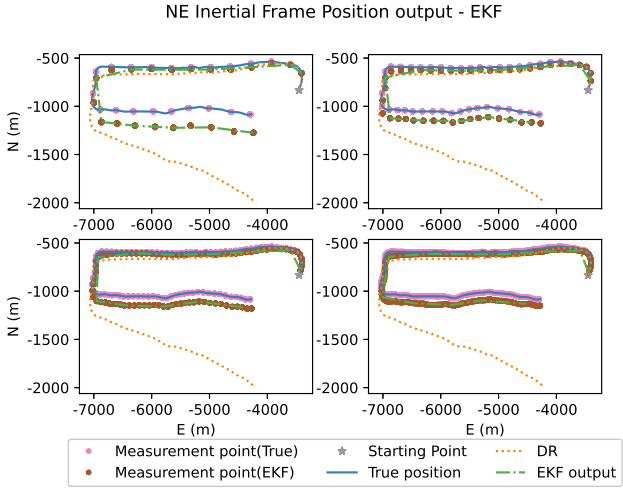

Fig. 5. EKF simulation result using (upper-left) 4 min, (upper-right) 2 min, (lower-left) 1 min, and (lower-right) 0.5 min arrival rate for each transmission segments with comparison to dead-reckoning (DR) method of inertial navigation method. The location of the beacon is in the origin.

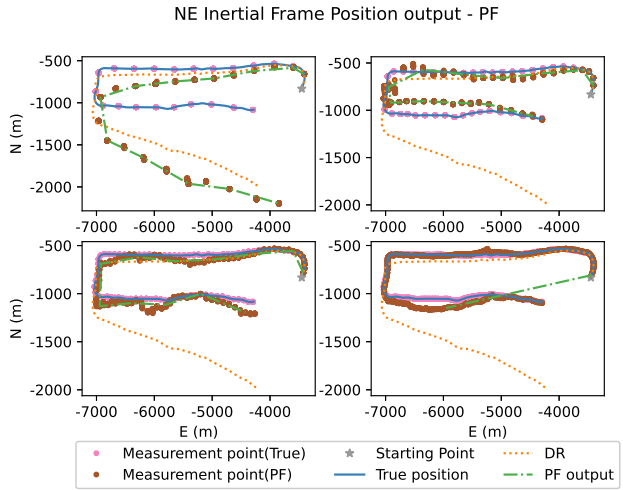

Fig. 6. PF simulation result using (upper-left) 4 min, (upper-right) 2 min, (lower-left) 1 min, and (lower-right) 0.5 min arrival rate for each transmission segments with comparison to dead-reckoning (DR) method of inertial navigation method. The location of the beacon is in the origin.

The EKF performance of the simulation is compared with state estimation carried out using a PF. Although an EKF algorithm offers low computational complexity, it may suffer from the linear approximation of the state model. On the other hand, a PF is a sequential Bayesian estimator that achieves asymptotic optimality as the number of particles increases. Due to its increasing computational cost with increasing number of particles, a PF is often not suitable for practical applications. However, it provides a benchmark for the performance of an EKF in the simulation environment. For our PF implementation, each particle is a state vector as defined in Section V. The particles are propagated forward using the state model every time the IMU measurements are taken. The weights for particles are computed using the observation equation in (14) and resampled according to these weights. The results shown in Fig. 6 used

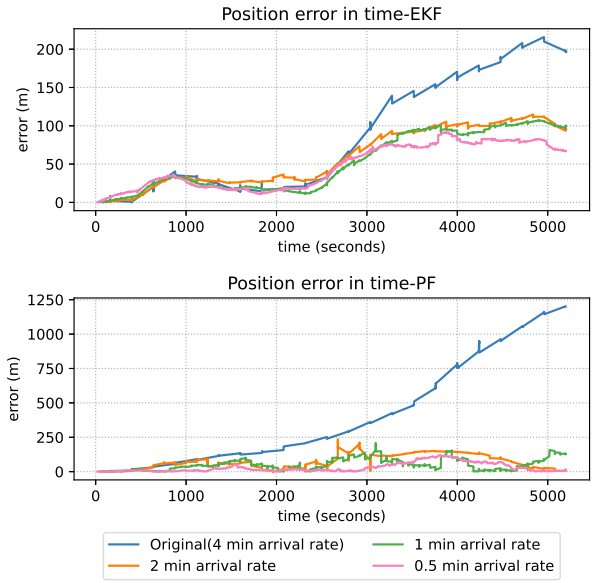

Fig. 7. Performance of EKF (top) and PF (bottom) with different acoustic segment arrival rate.

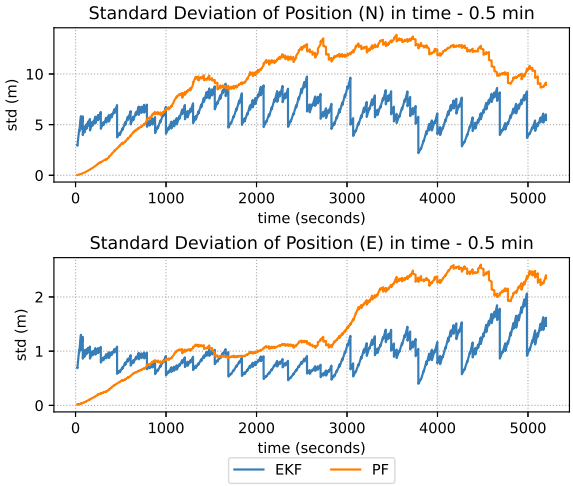

Fig. 8. Standard deviation of the estimated state from EKF and PF in (a) N-coordinate and (b) E-coordinate for 0.5 minute transmission interval.

20,000 particles for this simulation and Fig. 7 shows the position error in distance for each transmission interval. In Fig. 8 the standard deviations of EKF positions are computed by taking the square root of the diagonal components of the a posteriori estimate covariance matrix that corresponds to position vector in NE-coordinates. For the PF, the standard deviations are computed statistically using the particles of the position coordinates. As shown in Fig. 8, and Fig. 9, despite the linearized state model approximation of the EKF, the performance closely matches that of the PF with a large number of particles.

VII. Discussion

The EKF and PF simulation results show that localization in 3 to 7 km range is possible with the noise statistics of symbol timing and Doppler factor estimated from Doppler compensated

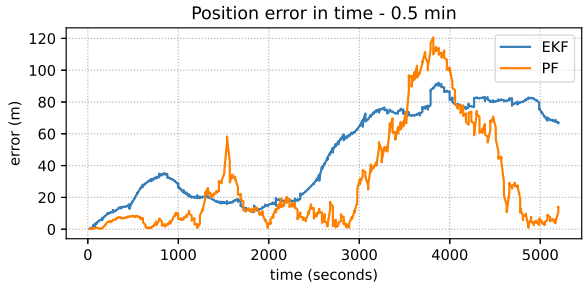

Fig. 9. Error in distance between the EKF and PF results and ground truth position for 0.5 minute transmission intervals.

DFE. From the Fig. 7, we observe that there are significant gains in accuracy from decreasing the arrival interval from 4 minutes to 2 minutes for both the EKF and PF. When the communication signal arrives more often than every 2 minutes, the results indicate that the observation rate is not the bottleneck for localization accuracy. In Fig. 4, the smallest singular value is independent of the arrival rate since the value is computed using a local observability gramian. However, for longer arrival intervals, the system state drifts away from the ground truth, so by the time the acoustic signal is available, the linearized local observability no longer holds.

In Fig. 8, we can observe that both algorithms generally show higher standard deviations for the position estimate in N-coordinate than those for the position estimate in E-coordinate. This indicates that the estimate has less uncertainty in its estimate in the radial direction since the N-coordinate difference between the track and the beacon ranges from 0.5 to 1 km whereas E-coordinate ranges from 3 to 7 km. The performance could be improved by placing the track and the beacon so that we have more variation in the azimuth between the vehicle and the beacon.

Although particle filtering achieves asymptotic optimality with increasing number of particles, the implementation is constrained by the memory size and computation power of the device running the algorithm. Due to this constraint, the particle number used in the simulation was set to 20,000 and the performance is suboptimal due to use of empirical results obtained with a limited number of particles for the proposal distribution. The results show similar performance between the EKF and PF, but PF simulation has the potential to outperform the EKF with advanced particle filtering techniques such as [24] and [25]. However such advanced filtering techniques are beyond the scope of this letter and left for future work.

The significance of this work lies in showing the feasibility of having a simultaneous acoustic communication-localization system on an AUV equipped with just a point-to-point communication system and inexpensive sensors such as an IMU and a barometer. The high data rate provided by the broadband acoustic communication system allows room for using information from various external sensors without power hungry, bulky equipment on the AUV. Further work involves incorporating the spatially varying sound-speed profile into the system. In addition to introducing uncertainty to the unit conversion between the time-of-flight to distance measurements, the varying speed of

sound bends the trajectory of the acoustic waves. Such effects could be addressed using ray tracing methods for anisoptropic media.

VIII. Conclusion

This letter presented a positioning system to localize an AUV equipped with an acoustic communication system and onboard inertial navigation sensors. We developed a Bayesian filtering framework that uses the recovered Doppler factor as well as time-of-flight measurement obtained from broadband acoustic communication signals and fuses them with the inertial measurement, for localization of an AUV. The framework provides localization for a simple AUV set-up, only equipped with an acoustic communication system and low-cost MEMS IMU. The simulation results verified that the algorithm operation in simulation augmented with real-world data using different acoustic transmission segment rates in a long range communication setting and is comparable to the performance of a PF, which is asymptotically optimal. Given that the distance between the beacon and the vehicle ranges from 3 to 7 km, the performance of the EKF is within a reasonable range and is expected to improve when operating over shorter distances. However, due to the current pandemic and restrictions on travel, our work was constrained to leveraging existing data sets, and new experiments are left for future study. These results provide a strong foundation for the implementation of the presented methods on real-world AUVs.

References

[1] R. Diamant, A. Feuer, and L. Lampe, "Choosing the right signal: Doppler shift estimation for underwater acoustic signals," in *Proc. 7th ACM Int. Conf. Underwater Netw. Syst.*, New York, NY, USA: Assoc. Comput. Machinery, 2012, pp. 1–8.

[2] M. Johnson, L. Freitag, and M. Stojanovic, "Improved doppler tracking and correction for underwater acoustic communications," in *Proc. IEEE Int. Conf. Acoust., Speech, Signal Process.*, 1997, vol. 1, pp. 575–578.

[3] T. Riedl and A. Singer, "Must-read: Multichannel sample-by-sample turbo resampling equalization and decoding," in *Proc. MTS/IEEE OCEANS - Bergen*, 2013, pp. 1–5.

[4] R. Diamant, L. M. Wolff, and L. Lampe, "Location tracking of ocean-current-related underwater drifting nodes using doppler shift measurements," *IEEE J. Ocean. Eng.*, vol. 40, no. 4, pp. 887–902, Oct. 2015.

[5] Z. Gong, C. Li, F. Jiang, and J. Zheng, "AUV-aided localization of underwater acoustic devices based on doppler shift measurements," *IEEE Trans. Wireless Commun.*, vol. 19, no. 4, pp. 2226–2239, Apr. 2020.

[6] E. Weinstein and A. Weiss, "Fundamental limitations in passive time-delay estimation—Part II: Wide-band systems," *IEEE Trans. Acoust., Speech, Signal Process.*, vol. ASSP-32, no. 5, pp. 1064–1078, Oct. 1984.

[7] T. J. Riedl and A. C. Singer, "Broadband doppler compensation: Principles and new results," in *Proc. Conf. Rec. 45th Asilomar Conf. Signals, Syst. Comput.*, 2011, pp. 944–946.

[8] M. B. Larsen, "Synthetic long baseline navigation of underwater vehicles," in *Proc. OCEANS MTS/IEEE Conf. Exhib. Conf.*, 2000, vol. 3, pp. 2043–2050.

[9] L. Paull, S. Saeedi, M. Seto, and H. Li, "AUV navigation and localization: A review," *IEEE J. Ocean. Eng.*, vol. 39, no. 1, pp. 131–149, Jan. 2014.

[10] J. González-García, A. Gómez-Espinosa, E. Cuan-Urquizo, L. G. García-Valdovinos, T. Salgado-Jiménez, and J. A. E. Cabello, "Autonomous underwater vehicles: Localization, navigation, and communication for collaborative missions," *Appl. Sci.*, vol. 10, no. 4, 2020, Art. no. 1256.

[11] Z. Li, S. E. Dosso, and D. Sun, "Motion-compensated acoustic localization for underwater vehicles," *IEEE J. Ocean. Eng.*, vol. 41, no. 4, pp. 840–851, Oct. 2016.

[12] Z. Yuyi, G. Zhenbang, W. Lei, Z. Ruiyong, and L. Huanxin, "Study of underwater positioning based on short baseline SONAR system," in *Proc. Int. Conf. Artif. Intell. Comput. Intell.*, 2009, vol. 2, pp. 343–346.

[13] E. I. Sarda and M. R. Dhanak, "Launch and recovery of an autonomous underwater vehicle from a station-keeping unmanned surface vehicle," *IEEE J. Ocean. Eng.*, vol. 44, no. 2, pp. 290–299, Apr. 2019.

[14] R. M. Eustice, L. L. Whitcomb, H. Singh, and M. Grund, "Experimental results in synchronous-clock one-way-travel-time acoustic navigation for autonomous underwater vehicles," in *Proc. IEEE Int. Conf. Robot. Automat.*, 2007, pp. 4257–4264.

[15] S. E. Webster, R. M. Eustice, H. Singh, and L. L. Whitcomb, "Advances in single-beacon one-way-travel-time acoustic navigation for underwater vehicles," *Int. J. Robot. Res.*, vol. 31, no. 8, pp. 935–950, 2012.

[16] M. V. Jakuba, J. C. Kinsey, J. W. Partan, and S. E. Webster, "Feasibility of low-power one-way travel-time inverted ultra-short baseline navigation," in *Proc. OCEANS MTS/IEEE Washington*, 2015, pp. 1–10.

[17] N. R. Rypkema, E. M. Fischell, and H. Schmidt, "One-way travel-time inverted ultra-short baseline localization for low-cost autonomous underwater vehicles," in *Proc. IEEE Int. Conf. Robot. Automat.*, 2017, pp. 4920–4926.

[18] S. Singh, M. Grund, B. Bingham, R. Eustice, H. Singh, and L. Freitag, "Underwater acoustic navigation with the WHOI micro-modem," in *Proc. OCEANS*, 2006, pp. 1–4.

[19] Y. Wu, X. Ma, S. Yan, D. Yuan, and S. Zhang, "Doppler aided synthetic long baseline navigation for a fast-moving underwater vehicles," in *Proc. OCEANS - MTS/IEEE Kobe Techno-Oceans*, 2018, pp. 1–5.

[20] H. L. Van Trees, *Detection, Estimation, and Modulation Theory. Part I., Detection, Estimation, and Linear Modulation Theory*. New York, NY, USA: Wiley, 2001.

[21] S. Haykin, *Kalman Filtering and Neural Networks*, vol. 47. Hoboken, NJ, USA: Wiley, 2004.

[22] J. Farrell, *Aided Navigation: GPS With High Rate Sensors*. New York, NY, USA: McGraw-Hill, 2008.

[23] J. K. Hedrick and A. Girard, *Control of nonlinear dynamic systems*. Berkeley, CA, USA: University of California, 2015.

[24] C. Shen, M. J. Brooks, and A. Van Den Hengel, "Augmented particle filtering for efficient visual tracking," in *Proc. IEEE Int. Conf. Image Process.*, vol. 3, 2005, pp. 856–859.

[25] J. Yun, F. Yang, and Y. Chen, "Augmented particle filters," *J. Amer. Stat. Assoc.*, vol. 112, no. 517, pp. 300–313, 2017.